

## Bnip3 expression in the brain of an Alzheimer's disease rat model

Agalic Rodriguez-Duboc <sup>a,b</sup>, Sophia Tsu Velicer <sup>a,b</sup>, Asgeir Kobro-Flatmoen <sup>a,b,\*</sup>

<sup>a</sup> Kavli Institute for Systems Neuroscience, Norwegian University of Science and Technology (NTNU), Trondheim, Norway

<sup>b</sup> K. G. Jebsen Centre for Alzheimer's Disease, Norwegian University of Science and Technology (NTNU), Trondheim, Norway

### ARTICLE INFO

#### Keywords:

Alzheimer's disease  
Amyloid- $\beta$   
Neuroanatomical markers  
Neurometabolism  
Mitophagy  
Synaptic modulation

### ABSTRACT

High levels of pro-mitophagic BCL2 and adenovirus E1B 19-kDa-interacting protein 3 (Bnip3) was recently found selectively present in reelin-expressing entorhinal cortex layer II neurons (Re+ ECLII neurons) in wild-type rats. This population of neurons is known to be affected in Alzheimer's disease. We therefore characterized Bnip3 expression in the forebrain of the McGill-R-Thy1-APP rat model, with a particular emphasis on Re+ ECLII neurons, and tested for potential differences in expression in these neurons vis-à-vis wild-type rats. To this end, we immunohistochemically labeled the brains of 24 animals divided into ages 3, 12, and 18 months, and analyzed their brains by optical density measurements and visual characterizations. We found that high Bnip3 expression was restricted to dorsolateral Re+ ECLII neurons, and, like reelin, was gradually less expressed in those situated successively further ventromedially. Quantitative analyses revealed no significant changes in Bnip3 expression within neuronal somata of these neurons as a function of age or genotype. Conversely, model rats at ages 3 and 18 months, but not at 12 months, appeared to have increased Bnip3 expression in the hippocampal sublayers that contain Re+ ECLII neuronal terminals. For the rest of the forebrain the expression of Bnip3 was, broadly speaking, low or absent.

Our results may be taken to indicate that (1) while the A $\beta$  pathology of McGill-R-Thy1-APP rats does not substantially alter the expression of Bnip3, (2) the subtle changes in Bnip3 expression associated with the terminals of Re+ ECLII neurons might reflect alterations in mitochondrial turnover, possibly as a response to increased levels and/or altered conformations of intraneuronal A $\beta$ .

### Introduction

We recently discovered, through work on Wistar rats, that BCL2 and adenovirus E1B 19-kDa interacting protein 3 (Bnip3) has a unique, high expression in the major subset of entorhinal cortex (EC) layer II (LII) principal neurons that are also characterized by expressing reelin (Re+ ECLII neurons). Furthermore, we showed that the expression pattern of Bnip3 closely matches the expression of reelin, with both proteins being highly expressed in ECLII neurons located close to the rhinal fissure (i.e. dorsolaterally), and having a gradually lower expression in neurons located successively further away from the rhinal fissure (i.e. ventromedially) (Omholt et al., 2024). Since a main function of Bnip3 is to induce mitophagy (Zhang et al., 2016; Rikka et al., 2011; Bellot et al., 2009), its unique expression in Re+ ECLII neurons likely reflects the very high metabolic turnover of these cells (Omholt et al., 2024).

Given the prominent role of mitochondrial impairments in the development of Alzheimer's disease (AD) (Kobro-Flatmoen et al., 2021), we decided to investigate whether the expression of Bnip3 is altered in

the context of AD-related pathology. We used the McGill-R-Thy1-APP rat model (hereafter referred to as McGill rats), which was generated on a Wistar background and has an extended phase of intraneuronal A $\beta$  (iA $\beta$ ) build-up, followed by amyloid plaque deposition starting from 6–9 months (Kobro-Flatmoen et al., 2016; Iulita et al., 2014), and characterized Bnip3 expression throughout the forebrain. Given the unique expression of Bnip3 in wild-type rats and their well-known vulnerability to the earliest pathological changes associated with AD (Kobro-Flatmoen et al., 2021), we paid particular attention to Re+ ECLII neurons.

Our main findings are that: (1) like wild type Wistar rats (hereafter referred to as WT rats), McGill rats have a high expression of Bnip3 that is restricted to Re+ ECLII neurons and matches the gradient of reelin expression. Furthermore, (2) we find no apparent change in Bnip3 expression in the somata of Re+ ECLII neurons as a function of age or genotype. However, (3) in McGill rats, Bnip3 expression appears higher in the hippocampal areas covered by the Re+ ECLII neuronal terminal fields at 3 and 18 months compared with the WT rats, while levels were similar between the 12-month groups. For the rest of the forebrain, we

\* Correspondence to: Olav Kyrres Gate 9, 7030 Trondheim, Norway.

E-mail address: [asgeir.kobro-flatmoen@ntnu.no](mailto:asgeir.kobro-flatmoen@ntnu.no) (A. Kobro-Flatmoen).

observed no substantial difference in Bnip3 expression in neuronal somata as a function of age or genotype by visual inspection of immunoenzyme-labeled sections.

Based on these results we discuss the possibility that the increased levels of Bnip3 in Re+ ECLII synaptic terminals seen in McGill rats could represent a response to cellular stress, potentially reflecting subtle mitochondrial stress brought on by the increased levels and/or altered conformations of iA $\beta$ .

## Methods

**Animal model.** This study used 24 rats, including 12 McGill rats (all homozygote for the transgene; six females and six males) and 12 outbred WT Wistar Han rats (three females and nine males). We analyzed the rats at three age-points, namely 3, 12, and 18 months, with each age-point including 4 McGill rats and 4 WT rats. The groups were not balanced for sex (WTs: 3-month-group had one female and three males; 12-month-group had one female and three males; 18-month-group had four females; McGill rats: 3-month-group had one female and three males; 12-month-group had two female and two males; 18-month-group had four males). Each procedure was authorized by the Norwegian Animal Research Authority and adhere to the European Convention for the Protection of Vertebrate Animals used for Experimental and Other Scientific Purposes. All animals were maintained on a 12-hour light/dark cycle in a regular housing climate (19–22 °C, 50–60 % humidity), with free access to water and food.

**Processing and immunohistochemistry.** A step-by-step description of tissue processing, immunohistochemistry and antibodies used can be found in Omholt et al. (2024). In brief, the animals were transcardially perfused, the brains were extracted and sectioned, and then immunolabeled.

**Imaging and quantification.** We scanned the tissue sections on a Zeiss Axio Scan.Z1 automated scanner system using a 20x objective (Plan-Apochromat 20x/0.8 M27) and identical settings throughout the study. Observations were then made using Zen software (version 2.6, Blue Ed.), alongside visual inspections through the ocular of a conventional Zeiss Axio Imager M1 microscope. For the double-immunofluorescence, the images were generated using Zen software, while the overlays were made in Photoshop (release 22.5.1). For quantifications of neuronal somata (all done in EC), we used five scanned sections per animal, taken from corresponding levels where the maximal dorsolateral-to-ventromedial extent of both lateral and medial entorhinal cortices (LEC and MEC, respectively) was obtained. This was done on 24 animals (12 McGill rats and 12 WT rats, 4 in each age group per genotype). The scanned sections were imported into QuPath (version 0.5.0) and, for each section, layer II of LEC or MEC was delineated. Using a subset of sections, we then calibrated the cell detection feature in QuPath to detect Bnip3-positive somata, and these settings were used for the automated quantification of optical densities (OD) in all animals. On each individual section, a background measurement was taken from deep layer I and subtracted from the raw values. The quantifications of the Bnip3 signal in the Re+ ECLII neuronal terminal fields in the hippocampus were done on the same 24 animals (again, 12 McGill rats and 12 WT rats, 4 in each age group per genotype). Here, for each animal, we used 7–8 sections, covering the dorsal one-third of the hippocampal septotemporal axis (these hippocampal sections were equally spaced out between Bregma level –1.92 to –4.44). On these sections we delineated the fields innervated by Re+ ECLII neuronal terminals, specifically, the outer and middle molecular layers of the dentate gyrus along with stratum lacunosum moleculare of CA3 and CA2 (cornu Ammonis 3/2). To quantify the putative Bnip3 signal from Re+ ECLII neuronal terminals we used the intensity feature computation tool in QuPath and obtained mean values of the signal of the delineated fields per section. On each individual hippocampal section, a background measurement was taken from the non-ECLII-innervated inner molecular layer of the dentate gyrus. As in the EC sections, the background values were then

subtracted from the raw values of each associated hippocampal section.

**Controlling for background labeling by the secondary antibodies.** As a control for the possibility of excessive background signal from our secondary antibodies, we labeled tissue across age groups while leaving out the primary antibody in parallel runs. These experiments indicated that the background signal was minimal or absent (Fig. 1).

**Statistical analyses.** Statistical analyses were conducted within the R statistical computing environment (version 4.4.0). Model fitting used the "glmmTMB" package (Brooks et al., 2017). Model diagnostics used the "DHARMA" (for details, see: <https://CRAN.R-project.org/package=DHARMA>) and "performance" packages (Lüdecke et al., 2021). Data from image processing following DAB staining were modeled within the Generalized Linear Mixed Model (GLMM) framework, using a Gamma distribution with a log link function to account for the data's strict positivity and positive skewness, as well as random intercepts to account for pseudo-replication (Zimmerman et al., 2021).

We modeled the Optical Density (OD) of individual neuronal somata ( $Y_{ijk}$ ) using genotype, age, and brain area (LEC vs. MEC) as fixed effects, along with all their interactions (Fig. 4). To account for the hierarchical nature of the data, random intercepts were included for each rat (j) and for each tissue section (k) nested within each rat. This addresses baseline variability between animals and within-animal variability across sections. The mathematical formulation of this model is:

$$\begin{aligned} Y_{ijk} &\sim \text{Gamma}\left(\mu_{ijk}, \phi\right), \text{Var}(Y_{ijk}) = \phi\mu_{ijk}^2, \\ \log(\mu_{ijk}) &= \beta_0 \\ &+ \beta_{\text{Genotype}}(\text{genotype}_{ijk}) \\ &+ \beta_{\text{Age}}(\text{age}_{ijk}) \\ &+ \beta_{\text{Area}}(\text{area}_{ijk}) \\ &+ \beta_{\text{Genotype} \times \text{Age}}(\text{genotype}_{ijk}, \text{age}_{ijk}) \\ &+ \beta_{\text{Genotype} \times \text{Area}}(\text{genotype}_{ijk}, \text{area}_{ijk}) \\ &+ \beta_{\text{Age} \times \text{Area}}(\text{age}_{ijk}, \text{area}_{ijk}) \\ &+ \beta_{\text{Genotype} \times \text{Age} \times \text{Area}}(\text{genotype}_{ijk}, \text{age}_{ijk}, \text{area}_{ijk}) \\ &+ b_{\text{rat}[j]} + b_{\text{rat:section}[j,k]}, \\ b_{\text{rat}[j]} &\sim \mathcal{N}(0, \sigma_{\text{rat}}^2), \\ b_{\text{rat:section}[j,k]} &\sim \mathcal{N}(0, \sigma_{\text{rat:section}}^2). \end{aligned}$$

Which corresponds to the R formula:  $od \sim \text{genotype} * \text{age} * \text{area} + (1 | \text{rat} / \text{section})$ .

To assess the effect of genotype regardless of age, we pooled data points from all ages and areas, keeping the same random effect structure, resulting in a simpler model with only genotype as a fixed effect (Supplementary figure). This simplified model's equation can be written as:

$$\begin{aligned} Y_{ijk} &\sim \text{Gamma}\left(\mu_{ijk}, \phi\right), \text{Var}(Y_{ijk}) = \phi\mu_{ijk}^2, \\ \log(\mu_{ijk}) &= \beta_0 \\ &+ \beta_{\text{Genotype}}(\text{genotype}_{ijk}) \\ &+ b_{\text{rat}[j]} \\ &+ b_{\text{rat:section}[j,k]}, \\ b_{\text{rat}[j]} &\sim \mathcal{N}(0, \sigma_{\text{rat}}^2), \\ b_{\text{rat:section}[j,k]} &\sim \mathcal{N}(0, \sigma_{\text{rat:section}}^2). \end{aligned}$$

Which corresponds to the R formula:  $od \sim \text{genotype} + (1 | \text{rat} / \text{section})$ .

To model the OD of the terminal fields ( $Y_{ij}$ ), the fixed effects included genotype, age, and their interaction (Fig. 5). A random intercept for each rat (j) was included to account for inter-animal variability. The mathematical formulation of this model is:

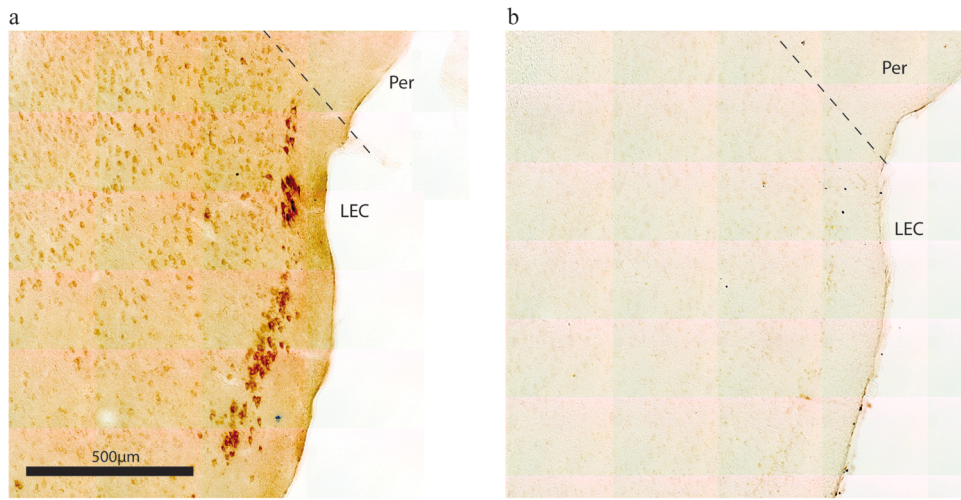


**Fig. 1.** No evident background labeling in our setup. (a) Immunolabeling with the Bnip3 antibody reveals a high level of signal in LEC layer II of McGill rats (example from an 18-month-old animal). (b) Immunolabeling without the Bnip3 antibody, keeping all else equal, produced a near complete absence of signal. The same is the case across the age groups. Scale bar indicated in figure (a) also applies to (b). Dashed lines marks border between LEC and Per. Abbreviations: LEC = Lateral entorhinal cortex; Per = Perirhinal cortex.

$$\begin{aligned}
 Y_{ij} &\sim \text{Gamma}\left(\mu_{ij}, \phi\right), \text{Var}(Y_{ij}) = \phi\mu_{ij}^2, \\
 \log(\mu_{ij}) &= \beta_0 \\
 &+ \beta_{\text{Genotype}}(\text{genotype}_{ij}) \\
 &+ \beta_{\text{Age}}(\text{age}_{ij}) \\
 &+ \beta_{\text{Genotype} \times \text{Age}}(\text{genotype}_{ij}, \text{age}_{ij}) \\
 &+ b_{\text{rat}[j]}, \\
 b_{\text{rat}[j]} &\sim \mathcal{N}(0, \sigma_{\text{rat}}^2).
 \end{aligned}$$

Which corresponds to the R formula:  $od \sim \text{genotype} * \text{age} + (1 | \text{rat})$ .

For all models, categorical predictors were dummy-coded with a reference level: genotype (Wild-Type) and age (3 months).

Statistical testing (expected marginal means and contrasts) was conducted with the "emmeans" package (for details, see: <https://CRAN.R-project.org/package=emmeans>). Post-hoc contrasts of the estimated marginal means were computed on the model's link scale using Wald z-tests. Given the confirmatory nature of our primary hypotheses, we chose to control the Family-Wise Error Rate (FWER) to minimize the risk of Type I errors. Accordingly, p-values from all contrasts were adjusted using the sequential Holm-Bonferroni method, and an adjusted p-value  $< 0.05$  was considered significant.

## Results

### Bnip3 has a strong expression in layer II of the entorhinal cortex

In line with our recently published findings concerning WT rats (Omholt et al., 2024) and prior reports (He et al., 2019; Lu et al., 2014; Zhang et al., 2011; Althaus et al., 2006), we found the expression of Bnip3 in McGill rats to be barely visible in cellular somata in most forebrain structures. Also in concordance with previous results in WT rats (Omholt et al., 2024), a major population of neurons located in ECLII in the domain close to the rhinal fissure expressed high levels of Bnip3, a feature which was present across all age groups examined. Moreover, for both LEC and MEC we found the same gradient as that reported in WT rats with respect to the expression level of Bnip3, namely a high expression in LII-neurons located close to the rhinal fissure (dorsolaterally) and gradually lower expression in LII-neurons located successively further away from the rhinal fissure (ventromedially; Fig. 2).

### Entorhinal Bnip3 expression is restricted to Re+ ECLII neurons

We recently reported that in WT rats, the expression of Bnip3 is restricted to Re+ ECLII neurons (Omholt et al., 2024). We therefore examined whether this is also the case in McGill rats. And, like in WT rats, double-immunolabeling against Bnip3 and reelin in McGill rats revealed that Bnip3 expression is restricted to Re+ ECLII neurons, and exhibits the same gradient as observed for reelin (Fig. 3).

### No apparent change in Bnip3 expression by age or genotype

Given the importance of EC in the context of AD, we decided to attempt to quantify the Bnip3 expression in Re+ ECLII neuronal somata. Specifically, analyzing LEC vs MEC separately, we investigated possible changes in Bnip3 expression as a function of age or genotype by quantifying the OD of the DAB-signal in neuronal somata in McGill rats compared with WT rats (4 rats per genotype per age-point, including 3, 12, and 18 months). We found no statistically significant changes (0.05 significance level) associated with neither age nor genotype (Fig. 4; see also supplementary figure).

### Bnip3 expression in hippocampal terminal fields of Re+ ECLII neurons varies with age

As synaptic changes are thought to arise prior to changes in their originating somata, we also quantified Bnip3 expression in the hippocampal fields in which Re+ ECLII neurons have their terminals, namely the outer and middle molecular layers of DG and stratum lacunosum moleculare of CA3 and CA2. This revealed that the expression level of Bnip3 in the hippocampal Re+ ECLII neuronal terminal fields was likely higher in the McGill rats at 3 months, given the clear statistical trend, and at 18 months where the increase was statistically significant compared with the WT rats at these ages, while levels were similar between the 12-month groups (Fig. 5).

### Bnip3 expression in other forebrain neurons is similar between the genotypes

The expression of Bnip3 in forebrain neurons outside of EC in McGill rats is likewise concordant with that found in WT rats (Omholt et al., 2024). Thus, moderate levels of Bnip3 are found in LII-neurons of the piriform cortex, while the preoptic nucleus has neurons reaching

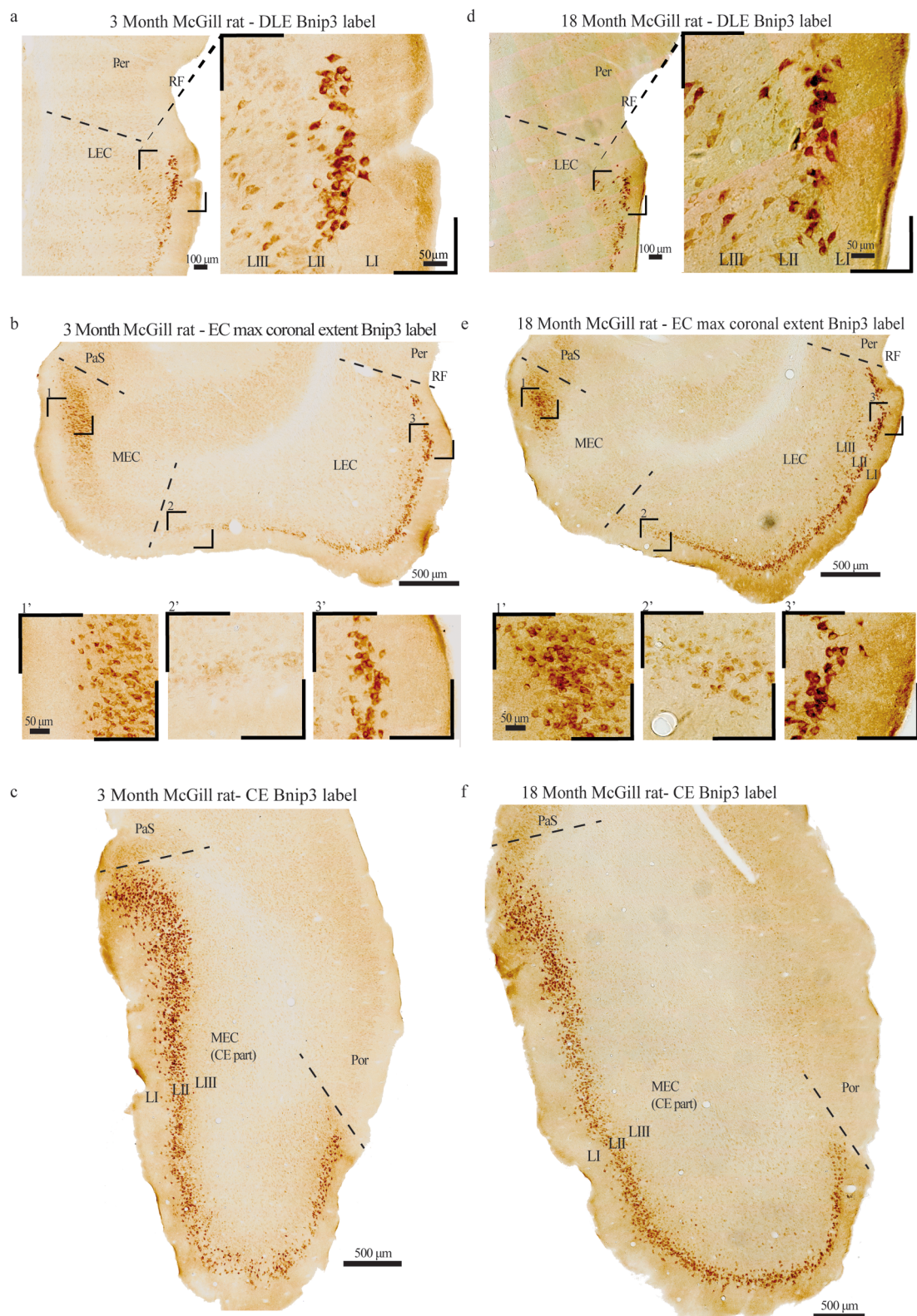


**Fig. 2.** A major population of ECLII neurons expresses Bnip3. (a) Image of the dorsolateral part of LEC (corresponding to the cytoarchitectonically defined ‘dorsolateral EC’) in a 3-month-old McGill rat, in which a major population of LII-neurons expresses high Bnip3 levels. (b) For both LEC and MEC (3-month-old McGill rat) the Bnip3-expression gradually decreases at positions successively further away from the rhinal fissure (RF; note that RF partly wraps around the posterior part of the brain, hence, like for the dorsal part of LEC, the dorsal part of MEC is closer to RF relative to the ventral part). (c) Image of the ‘caudal extreme’ of EC in coronal sections taken from a 3-month-old McGill rat, at which level MEC is located relatively close to RF. (d–f) Corresponding images for 18-month-old animals. Abbreviations: DLE = Dorsolateral entorhinal cortex; ECLII = Entorhinal cortex layer II; LEC = Lateral entorhinal cortex; MEC = Medial entorhinal cortex; PaS = Parasubiculum; Per = Perirhinal cortex; Por = Posterior rhinal fissure. Scale bars are indicated for each figure, note that for the insets in (b) and (e) the scale bar in the leftmost inset applies to the two associated insets.

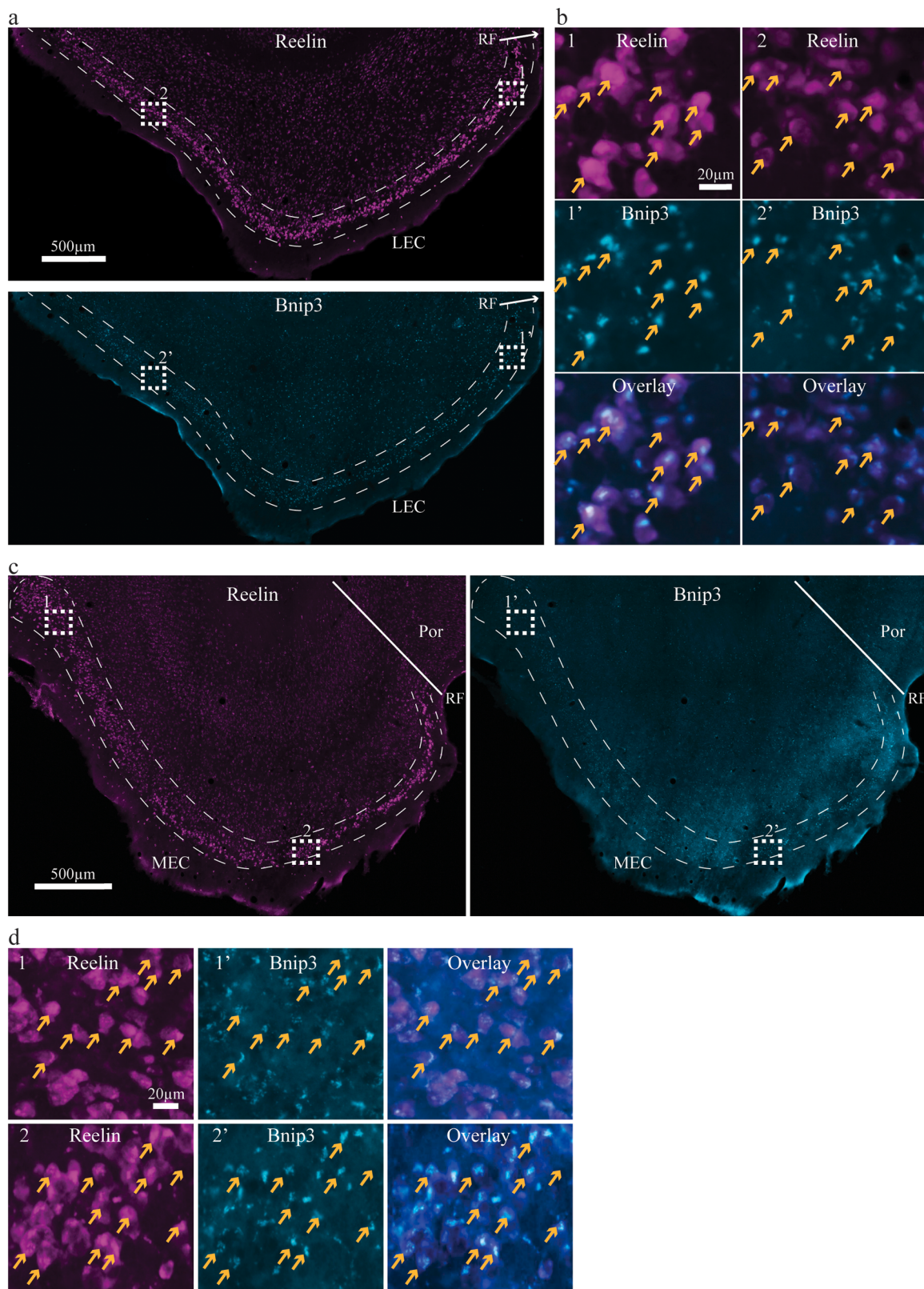


**Fig. 3.** Entorhinal Bnip3-expression is restricted to Re+ ECLII neurons. (a) LEC: The top panel displays labeling for reelin while the lower panel displays labeling for Bnip3. (b) LEC: Higher powered insets from (a), numbered based on their location, show that Bnip3 is restricted to Re+ ECLII neurons- and follows the same gradient as reelin, thus having a high expression in neurons close to the rhinal fissure (RF) and a gradually lower expression in neurons situated successively further away from RF. (c) MEC: The left panel displays labeling for reelin while the right panel displays labeling for Bnip3. (d) MEC: Higher powered insets from (c), numbered based on their location, shows that Bnip3 is restricted to Re+ ECLII neurons. Arrows point to examples of neurons that co-express Bnip3 and reelin. Scale bars: (a, top panel) also applies to (a, lower panel); (b, top left) applies to all in (b); (c, left panel) also applies to (c, right panel); and (d, top left) applies to all in (d). Dashed lines delimit ECLII. Abbreviations: ECLII = Entorhinal cortex layer II; LEC = Lateral entorhinal cortex; MEC = Medial entorhinal cortex; Por = Postrhinal cortex.

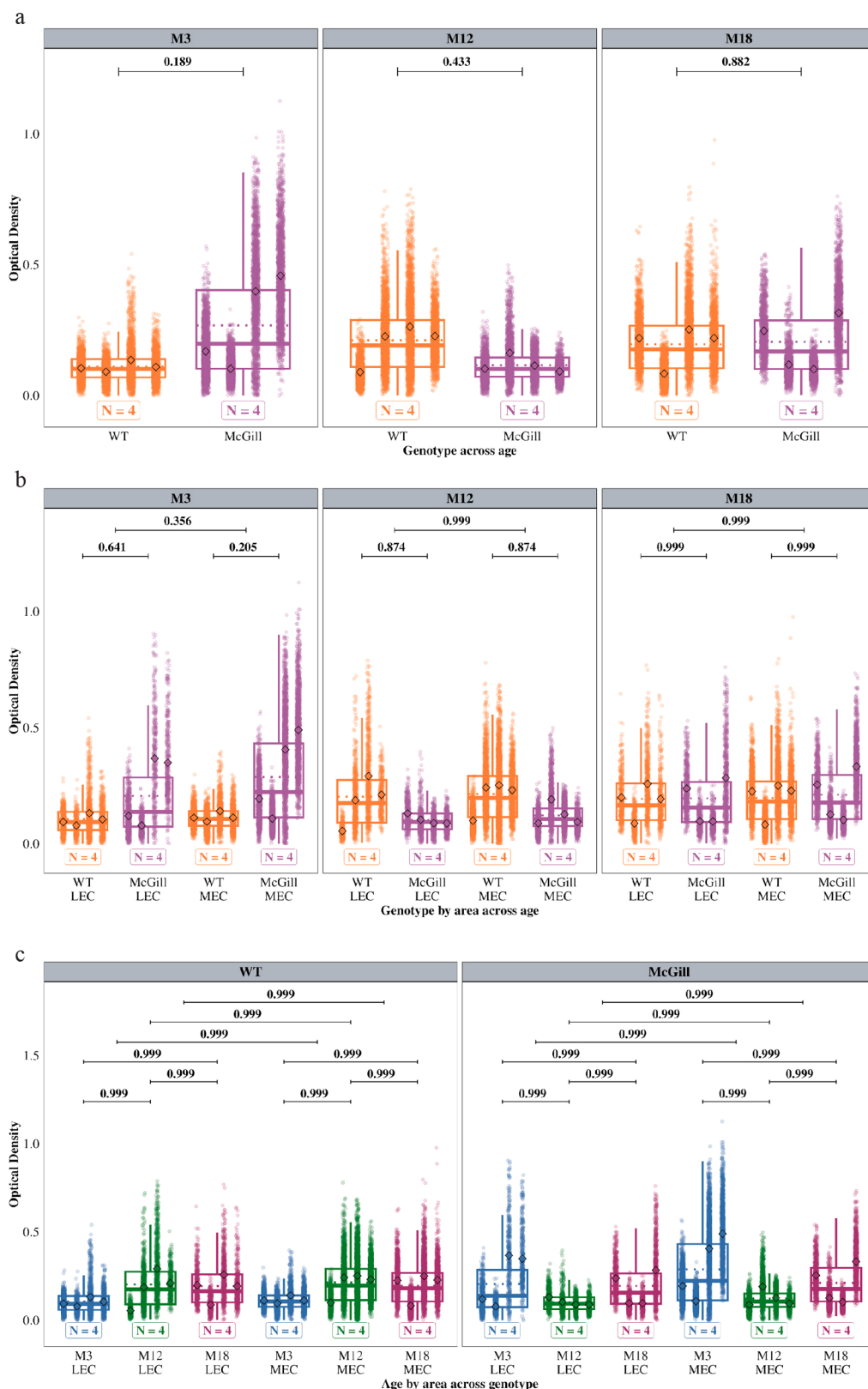


**Fig. 4.** Quantification of Bnip3-expression in Re+ ECLII neuronal somata indicates no difference by genotype or age. (a) No difference in Bnip3-levels (optical density) was detected in Re+ ECLII somata (combining LEC and MEC) between McGill rats and WT rats in our age groups (3, 12, and 18 months). (b) The same result is evident from an interaction plot showing differences within LEC and MEC across the age groups. (c) Likewise, an interaction plot where we tested for differences between LEC or MEC for each genotype across the age groups shows no statistical difference in Bnip3 levels. Diamond shapes indicate the number of animals in each experimental group ( $n = 4$ ), while the transparent dots represent the individual neuronal somata. Each column of transparent dots corresponds to an individual rat. The p-values are indicated above the plots. Abbreviations: ECLII = Entorhinal cortex layer II; LEC = Lateral entorhinal cortex; MEC = Medial entorhinal cortex; M = age of rats in months; WT = Wild type animals.

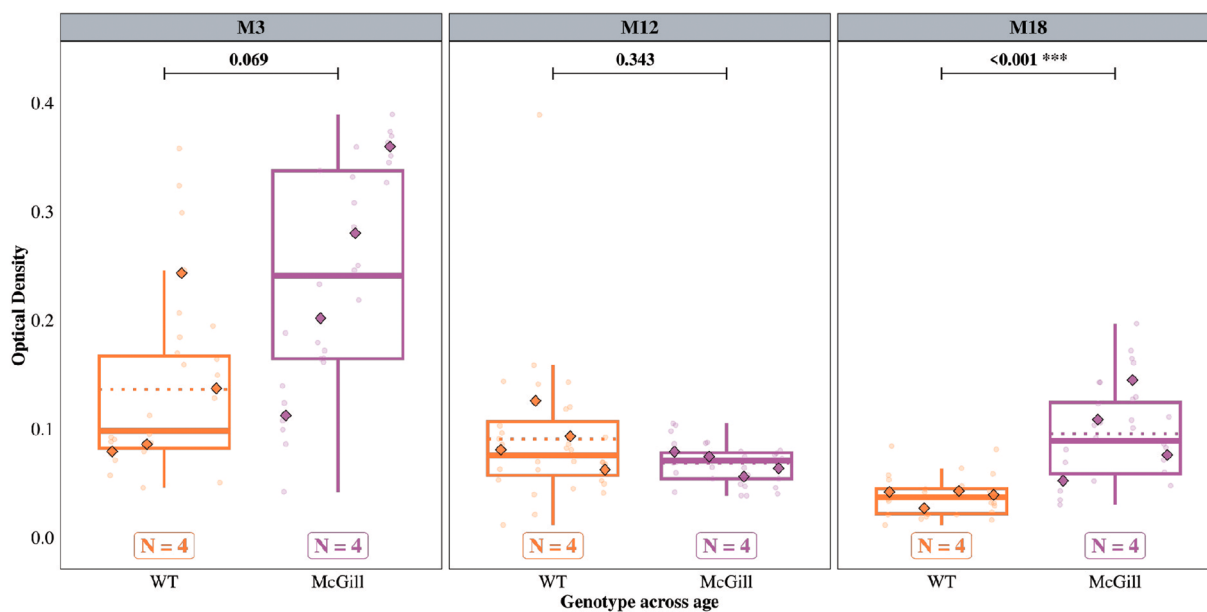


**Fig. 5.** Bnip3 expression in hippocampal terminal fields of Re+ ECLII neurons varies with age. Quantification of Bnip3-expression in the hippocampal fields in which Re+ ECLII neurons have their terminals (DG, CA3 and CA2, combined) revealed a trend toward a higher level in 3-month-old McGill rats (3 M, leftmost panel) and a significant increase in 18-month-old (18 M, rightmost panel) McGill rats, both compared with WT rats. For 12-month-old animals (12 M, middle panel) the levels were similar between the groups. Diamond shapes indicate the number of animals in each experimental group ( $n = 4$ ), while the transparent dots represent individual field measurements (one measurement per section) of Re+ ECLII terminal fields across DG, CA3, and CA2. Each column of transparent dots corresponds to an individual rat. The p-values are indicated above the plots. Abbreviations: DG = Dentate gyrus; CA3/2 = cornu Ammonis 3/2; ECLII = Entorhinal cortex layer II; M = age of rats in months; WT = Wild type animals.

moderate and occasionally even high levels (Fig. 6a). Broadly speaking, the expression of Bnip3 in the hippocampal formation is low or absent, though field CA3 constitutes an exception, having a moderate level of Bnip3 expression in pyramidal-layer neurons. However, as is relevant to the above section, a marked increase is present in the neuropil of the outer and middle molecular layers of DG and stratum lacunosum moleculare of CA3 and CA2, matching the locations of the ECLII terminal fields. And, as in WT rats, the labeling relating to the DG is more pronounced in the free (lower) blade (Fig. 6b). Subsets of neurons with low to moderate levels of Bnip3 expression are furthermore present in parts of the visual cortex (Fig. 6c), the retrosplenial, motor, and somatosensory cortices (Fig. 6d), and in the frontal cortex (Fig. 6e).

## Discussion

Here we investigated whether the expression of the pro-mitophagic protein Bnip3 is altered by AD-related changes as present in McGill rats. As in WT rats (Omholst et al., 2024), we find that the expression of Bnip3 is restricted to Re+ ECLII neurons, that it is particularly high in those located close to the rhinal fissure (dorsolaterally), and that the expression becomes gradually lower in Re+ ECLII neurons located successively further away from the rhinal fissure (ventromedially). The gradient of Bnip3 expression thus corresponds to the gradient of reelin in these neurons (Kobro-Flatmoen et al., 2016).

We observed no substantial difference in Bnip3 expression in neuronal somata as a function of age or genotype in the forebrain of McGill rats relative to WT rats by visual inspection of immunoenzyme-labeled sections. Likewise, quantification of the optical density of Re+ ECLII neuronal somata produced similar results between the two genotypes, as well as across the different age groups. However, in the hippocampal fields where Re+ ECLII neurons have their terminals, we detected considerably higher levels of Bnip3 expression in the McGill rats at 3 (non-statistically significant) and 18 months (statistically significant) compared with the WT rats at these ages, while levels were similar between the groups at 12 months. These subtle changes appear

in keeping with the relatively modest pathological changes reported for McGill rats.

Since stereological investigations have revealed minor neuron loss only in the subiculum of homozygous rats by 18 months of age (Heggland et al., 2015), little-to-no neurodegeneration appears to occur in McGill rats. Nevertheless, impairments exist, including several that emerge before amyloid plaques form that are instead associated with iA $\beta$  in neurons. For example, proteins involved in synaptic plasticity exhibit an early decline (Do Carmo et al., 2018). Furthermore, the model presents with subtle neuronal metabolic deficiencies, including reduced mitochondrial bioenergetic capacity and reduced tricarboxylic acid cycle turnover (Nilsen et al., 2014; Adami et al., 2017). Oxidative stress is likely a key player in this (Adami et al., 2017), not least since an increased expression of genes responsive to oxidative stress and DNA damage was found at pre-plaque stages in this model (Foret et al., 2024). These findings appear consistent with the memory impairments reported to affect the model at pre-plaque stages, which have been established for spatial- and working memory (Galeano et al., 2014), novel object recognition, and fear conditioning paradigms (Iulita et al., 2014).

Re+ ECLII neurons appear to be the only cortical population of neurons expressing a high level of Bnip3, at least in rats. The Bnip3 expression in these neurons coincides with that of reelin, and, as mentioned above, the expression of both proteins reaches its highest levels in neurons located close to the rhinal fissure, and gradually decreases in those located successively further away from the rhinal fissure. This feature, along with the facts that reelin is a canonical synaptogenic protein (Niu et al., 2004) whose function includes the remodeling of synaptic contacts (Bosch et al., 2016), and that Re+ ECLII neurons have extremely large dendritic trees (Canto and Witter, 2012), indicate that these neurons are subject to a very high demand for synaptic plasticity that requires a particularly high level of mitochondrial turnover (Omholst et al., 2024).

The lack of observable differences in Bnip3 expression in neuronal somata as a function of age or genotype, including in Re+ ECLII neurons

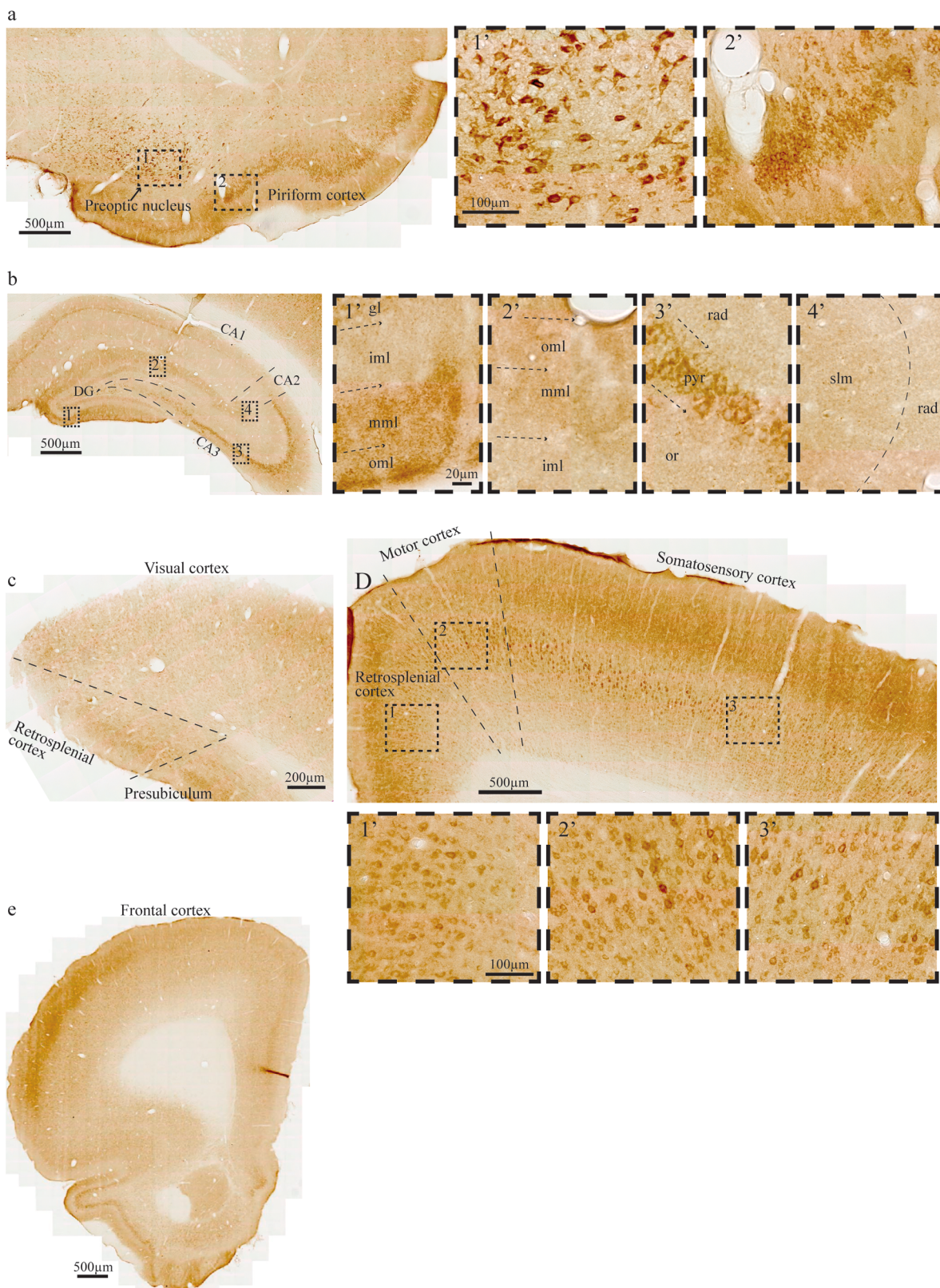


**Fig. 6.** Moderate Bnip3-expression observed in certain structures outside of the entorhinal cortex. (a) Neuronal somata in the piriform cortex and the preoptic nucleus contain moderate levels of Bnip3, and, in the case of the latter structure, even occasionally high levels. (b) Moderately expressing neurons are also found in CA3 (note also the labeled neuropil in the outer  $\frac{2}{3}$  of the molecular layer of DG (mml and oml), and the less clearly labeled neuropil in the outer  $\frac{2}{3}$  of stratum lacunosum-moleculare (slm) in CA3 and CA2), in (c) the visual cortex, (d) the retrosplenial, motor, and somatosensory cortices, and (e) the frontal cortex. Scale bars are indicated in each figure, note that for the related insets, the leftmost scale bar applies to all. Abbreviations: DG = Dentate gyrus; CA3/2/1 = cornu Ammonis 3/2/1; gl = granular layer of dentate gyrus; iml = inner molecular layer of dentate gyrus; mml = middle molecular layer of dentate gyrus; oml = outer molecular layer of dentate gyrus; pyr = stratum pyramidale; rad = stratum radiatum; slm = stratum lacunosum-moleculare; or = stratum oriens.

for which we quantified the optical densities, suggests that the homeostatic regulation of Bnip3 in somata is maintained in both McGill and WT rats, at least up to 18 months. On the other hand, the fact that the 3- and 18-month-old groups displayed higher levels of Bnip3 in McGill rats compared with WT rats in the outer and middle molecular layers of DG and stratum lacunosum moleculare of CA3 and CA2 indicates that subtle changes may be affecting these neurons. McGill rats express increased levels of iA $\beta$  in forebrain neurons, including ECLII neurons, and this is detectable from one week postnatal. By 6 months of age the levels of iA $\beta$  are relatively high, but around the time extracellular A $\beta$ -plaques start to appear – between 6–9 months – levels of iA $\beta$  have been reported to drop (Iulita et al., 2014; Leon et al., 2010). This is consistent with findings that levels of iA $\beta$  are affected by levels of extracellular A $\beta$ , which likely involves A $\beta$ -driven stimulation of  $\beta$ -cleavage to alter A $\beta$  production (Roos et al., 2021). One explanation may be that the increased level of Bnip3 in the hippocampal terminal fields of Re+ ECLII neurons in McGill rats reflects mitochondrial stress brought on by the increased levels of iA $\beta$  and/or altered forms of iA $\beta$  (Umeda et al., 2011). In this scenario, as A $\beta$ -plaques begin to form and levels of iA $\beta$  temporarily drop, it is at least conceivable that a consequent reduction in mitochondrial stress leads to a temporary normalization of Bnip3 expression in the hippocampal terminals at 12 months. Whether the observed increase in Bnip3 expression in McGill rats by 18 months reflects the accumulated extracellular A $\beta$ -plaque pathology, which affects both EC and hippocampal formation (Heggland et al., 2015), or whether it again reflects increased levels of iA $\beta$  driven by influx of plaque derived A $\beta$ , or even increased neuronal retention of iA $\beta$ , is at this point an open question. Clearly, further work, including larger- and gender balanced groups of animals, and hippocampal and EC layer- or even neuron-specific protein analyses will be needed to address these questions.

#### CRediT authorship contribution statement

**Asgeir Kobro-Flatmoen:** Writing – review & editing, Writing – original draft, Supervision, Project administration, Methodology, Investigation, Formal analysis, Conceptualization. **Sophia Tsu Velicer:** Writing – review & editing, Investigation, Formal analysis. **Agalie Rodriguez-Duboc:** Writing – review & editing, Writing – original draft, Methodology, Investigation, Formal analysis, Data curation, Visualization.

#### Consent to participate

Not applicable.

#### Consent for publication

Not applicable.

#### Ethical statement

All procedures in this study were approved by the Norwegian Animal Research Authority and follow the European Convention for the Protection of Vertebrate Animals used for Experimental and Other Scientific Purposes.

All work presented in this study represents original work that has not been published elsewhere, except as in poster format at scientific conferences. The manuscript is not under consideration for publication elsewhere and is approved by all authors.

We, the authors, confirm that we have no conflicts of interest in relation to the work presented in this manuscript.

#### Funding

This work was supported by a Center Grant from (1) The Liaison Committee for Education, Research and Innovation in Central Norway

(<https://www.helse-midt.no/samarbeidsorganet>), (2) The Department of Neurology and Clinical Neurophysiology, University Hospital of Trondheim, Trondheim, Norway, (3) The K. G. Jebsen Foundation (<http://www.kgjf.org/>), (4) The Kavli Foundation (<https://www.kavlifoundation.org/>), (5) The Kavli Institute for Systems Neuroscience, and (6) Nasjonalforeningen for Folkehelsen, grant number 35578. The funders had no role in the study design, data collection and analysis, decision to publish, or preparation of the manuscript.

#### Declaration of Competing Interest

We, the authors, confirm that we have no conflicts of interest in relation to the work presented in this manuscript.

#### Acknowledgments

We wish to thank Raissa Lejneva and Bruno Monterotti (1955–2024) for excellent technical assistance.

#### Appendix A. Supporting information

Supplementary data associated with this article can be found in the online version at doi:[10.1016/j.bramec.2025.202518](https://doi.org/10.1016/j.bramec.2025.202518).

#### Data availability

The data and code supporting the findings of this study are openly available in [Bnip3\_McGill\_AD] at [DOI: [10.5281/zenodo.15199696](https://doi.org/10.5281/zenodo.15199696)] (<https://doi.org/10.5281/zenodo.15199696>).

#### References

- Adami, P.V.M., Quijano, C., Magnani, N., et al., 2017. Synaptosomal bioenergetic defects are associated with cognitive impairment in a transgenic rat model of early Alzheimer's disease. *J. Cereb. Blood Flow. Metab.* 37, 69–84. <https://doi.org/10.1177/0271678X15615132>.
- Althaus, J., Bernaudin, M., Petit, E., et al., 2006. Expression of the gene encoding the pro-apoptotic BNIP3 protein and stimulation of hypoxia-inducible factor-1alpha (HIF-1alpha) protein following focal cerebral ischemia in rats, 20060207 *Neurochem. Int.* 48, 687–695. <https://doi.org/10.1016/j.neuint.2005.12.008>.
- Bellot, G., Garcia-Medina, R., Gounon, P., et al., 2009. Hypoxia-induced autophagy is mediated through hypoxia-inducible factor induction of BNIP3 and BNIP3L via their BH3 domains, 20090309 *Mol. Cell Biol.* 29, 2570–2581. <https://doi.org/10.1128/MCB.00166-09>.
- Bosch, C., Masachs, N., Exposito-Alonso, D., et al., 2016. Reelin regulates the maturation of dendritic spines, synaptogenesis and glial ensheathment of newborn granule cells. *Cereb. Cortex* 26, 4282–4298. <https://doi.org/10.1093/cercor/bhw216>.
- Brooks, M.E., Kristensen, K., van Benthem, K.J., et al., 2017. glmmTMB balances speed and flexibility among packages for zero-inflated generalized linear mixed modeling. *R. J.* 9, 378–400. <https://doi.org/10.32614/RJ-2017-066>.
- Canto, C.B., Witter, M.P., 2012. Cellular properties of principal neurons in the rat entorhinal cortex. I. The lateral entorhinal cortex, 20111207. DOI: *Hippocampus* 22, 1256–1276. <https://doi.org/10.1007/s10407-010-0997>.
- Do Carmo, S., Crynen, G., Paradis, T., et al., 2018. Hippocampal proteomic analysis reveals distinct pathway deregulation profiles at early and late stages in a Rat Model of Alzheimer's-like amyloid pathology, 20170513. DOI: *Mol. Neurobiol.* 55, 3451–3476. <https://doi.org/10.1007/s12035-017-0580-9>.
- Foret, M.K., Orciani, C., Welikovitch, L.A., et al., 2024. Early oxidative stress and DNA damage in Abeta-burdened hippocampal neurons in an Alzheimer's-like transgenic rat model, 20240714. DOI: *Commun. Biol.* 7, 861. <https://doi.org/10.1038/s42003-024-06552-4>.
- Galeano, P., Martino Adami, P.V., Do Carmo, S., et al., 2014. Longitudinal analysis of the behavioral phenotype in a novel transgenic rat model of early stages of Alzheimer's disease, 321. 20140916. DOI: *Front Behav. Neurosci.* 8. <https://doi.org/10.3389/fnbeh.2014.00321>.
- He, M., Xiang, Z., Xu, L., et al., 2019. Lipopolysaccharide induces human olfactory ensheathing glial apoptosis by promoting mitochondrial dysfunction and activating the JNK-Bnip3-Bax pathway, 20181029 *Cell Stress Chaperon.* 24, 91–104. <https://doi.org/10.1007/s12192-018-0945-7>.
- Heggland, I., Storkaas, I.S., Soligard, H.T., et al., 2015. Stereological estimation of neuron number and plaque load in the hippocampal region of a transgenic rat model of Alzheimer's disease, 20150325 *Eur. J. Neurosci.* 41, 1245–1262. <https://doi.org/10.1111/ejn.12876>.
- Iulita, M.F., Allard, S., Richter, L., et al., 2014. Intracellular Abeta pathology and early cognitive impairments in a transgenic rat overexpressing human amyloid precursor

- protein: a multidimensional study, 20140605 *Acta Neuropathol. Commun.* 2, 61. <https://doi.org/10.1186/2051-5960-2-61>.
- Kobro-Flatmoen, A., Nagelhus, A., Witter, M.P., 2016. Reelin-immunoreactive neurons in entorhinal cortex layer II selectively express intracellular amyloid in early Alzheimer's disease, 20160516. DOI: *Neurobiol. Dis.* 93, 172–183. <https://doi.org/10.1016/j.nbd.2016.05.012>.
- Kobro-Flatmoen, A., Lagartos-Donate, M.J., Aman, Y., et al., 2021. Re-emphasizing early Alzheimer's disease pathology starting in select entorhinal neurons, with a special focus on mitophagy, 20210220 *Ageing Res. Rev.* 67, 101307. <https://doi.org/10.1016/j.arr.2021.101307>.
- Leon, W.C., Canneva, F., Partridge, V., et al., 2010. A novel transgenic rat model with a full Alzheimer's-like amyloid pathology displays pre-plaque intracellular amyloid-beta-associated cognitive impairment, 2010/02/19 *J. Alzheimers Dis.* 20, 113–126. <https://doi.org/10.3233/JAD-2010-1349>.
- Lu, P., Kamboj, A., Gibson, S.B., et al., 2014. Poly(ADP-ribose) polymerase-1 causes mitochondrial damage and neuron death mediated by Bnip3, 2014/11/28 *J. Neurosci.* 34, 15975–15987. <https://doi.org/10.1523/JNEUROSCI.2499-14.2014>.
- Lüdecke, D., Ben-Shachar, M., Patil, I., et al., 2021. performance: an R package for assessment, comparison and testing of statistical models. *J. Open Source Softw.* 6. <https://doi.org/10.21105/joss.03139>.
- Nilsen, L.H., Witter, M.P., Sonnewald, U., 2014. Neuronal and astrocytic metabolism in a transgenic rat model of Alzheimer's disease, 20140305 *J. Cereb. Blood Flow. Metab.* 34, 906–914. <https://doi.org/10.1038/jcbfm.2014.37>.
- Niu, S., Renfro, A., Quattrochi, C.C., et al., 2004. Reelin promotes hippocampal dendrite development through the VLDLR/ApoER2-Dab1 pathway. *Neuron* 41, 71–84. [https://doi.org/10.1016/s0896-6273\(03\)00819-5](https://doi.org/10.1016/s0896-6273(03)00819-5).
- Omholt, S.W., Lejneva, R., Donate, M.J.L., et al., 2024. Bnip3 expression is strongly associated with reelin-positive entorhinal cortex layer II neurons. *Brain Struct. Funct.*, 20240625 <https://doi.org/10.1007/s00429-024-02816-1>.
- Rikka, S., Quinsay, M.N., Thomas, R.L., et al., 2011. Bnip3 impairs mitochondrial bioenergetics and stimulates mitochondrial turnover. *Cell Death Differ.* 18, 721–731.
- Roos, T.T., Garcia, M.G., Martinsson, I., et al., 2021. Neuronal spreading and plaque induction of intracellular Abeta and its disruption of Abeta homeostasis, 20210716 *Acta Neuropathol.* 142, 669–687. <https://doi.org/10.1007/s00401-021-02345-9>.
- Umeda, T., Tomiyama, T., Sakama, N., et al., 2011. Intraneuronal amyloid beta oligomers cause cell death via endoplasmic reticulum stress, endosomal/lysosomal leakage, and mitochondrial dysfunction in vivo, 20110412 *J. Neurosci. Res.* 89, 1031–1042. <https://doi.org/10.1002/jnr.22640>.
- Zhang, T., Xue, L., Li, L., et al., 2016. BNIP3 protein suppresses PINK1 kinase proteolytic cleavage to promote mitophagy. *J. Biol. Chem.* 291, 21616–21629. <https://doi.org/10.1074/jbc.M116.733410>.
- Zhang, Z., Shi, R., Weng, J., et al., 2011. The proapoptotic member of the Bcl-2 family Bcl-2 / E1B-19K-interacting protein 3 is a mediator of caspase-independent neuronal death in excitotoxicity, 20101201 *FEBS J.* 278, 134–142. <https://doi.org/10.1111/j.1742-4658.2010.07939.x>.
- Zimmerman, K.D., Espeland, M.A., Langefeld, C.D., 2021. A practical solution to pseudoreplication bias in single-cell studies, 20210202 *Nat. Commun.* 12, 738. <https://doi.org/10.1038/s41467-021-21038-1>.